

Cationic Polymer Modified Mesoporous Silica Nanoparticles for Targeted siRNA Delivery to HER2⁺ Breast Cancer

Worapol Ngamcherdtrakul, Jingga Morry, Shenda Gu, David J. Castro, Shaun M. Goodyear, Thanapon Sangvanich, Moataz M. Reda, Richard Lee, Samuel A. Mihelic, Brandon L. Beckman, Zhi Hu, Joe W. Gray,* and Wassana Yantasee*

In vivo delivery of siRNAs designed to inhibit genes important in cancer and other diseases continues to be an important biomedical goal. A new nanoparticle construct that is engineered for efficient delivery of siRNA to tumors is now described. The construct comprises a 47-nm mesoporous silica nanoparticle core coated with a crosslinked polyethyleneimine–polyethylene-glycol copolymer, carrying siRNA against the human epidermal growth factor receptor type 2 (HER2) oncogene, and coupled to the anti-HER2 monoclonal antibody (trastuzumab). The construct is engineered to increase siRNA blood half-life, enhance tumor-specific cellular uptake, and maximize siRNA knock-down efficacy. The optimized anti-HER2 nanoparticles produce apoptotic death in HER2 positive (HER2⁺) breast cancer cells grown in vitro, but not in HER2 negative (HER2⁻) cells. One dose of the siHER2–nanoparticles reduces HER2 protein levels by 60% in trastuzumab-resistant HCC1954 xenografts. Administration of multiple intravenous doses over 3 weeks significantly inhibits tumor growth ($p < 0.004$). The siHER2-nanoparticles have an excellent safety profile in terms of blood compatibility and low cytokine induction, when exposed to human peripheral blood mononuclear cells. The construct can be produced with high batch-to-batch reproducibility and the production methods are suitable for large-scale production. These results suggest that this siHER2-nanoparticle is ready for clinical evaluation.

are identifying genomic aberrations and affected regulatory networks that enable aspects of cancer progression including proliferation, angiogenesis, invasion, drug resistance, and metastasis.^[1] These discovery efforts and associated large-scale functional studies^[2] are guiding the development of a wide range of therapeutic agents designed to inhibit the genes and pathways on which cancers depend. Unfortunately, many of the most attractive therapeutic targets currently are not druggable using small molecule inhibitors or antibodies.^[3] RNA interference using siRNA is an attractive alternative to inhibiting otherwise intractable therapeutic targets.^[4] This strategy has been effective in vitro. However, delivery of siRNAs to tumors in patients is still challenging.

Several strategies to deliver siRNAs in vivo have involved packing siRNAs into nanoparticle (NP) constructs designed to increase siRNA half-life in the blood,^[5] allow escape from the reticuloendothelial system (RES) recognition that rapidly causes nanoparticles to accumulate in the liver and spleen,^[6] and enhance tumor-

specific cellular uptake. Many types of organic and inorganic nanoparticles have been evaluated as siRNA carriers to achieve these goals. These include viral-capsids, cyclodextrin, cationic polymers, gold nanoparticles, peptides (see reviews),^[7] and mesoporous silica nanoparticles (MSNPs, see reviews).^[8]

Several organic nanoparticles developed for anticancer agent delivery show promise, but limitations have been identified. For example, viral-based carriers sometimes induce adverse immune responses. Cationic lipid nanoparticles have shown efficacy in treating liver cancer^[9] since they home to the liver and spleen via RES recognition. Unfortunately, they did not show objective efficacy when used to treat tumors at other anatomic sites.^[10] In addition, they elicited hematological toxicity in some cases^[11] and some have been difficult to manufacture reproducibly at large scale. A cyclodextrin-based nanoparticle targeted to the human transferrin protein (hTf) was the first targeted siRNA delivery system to demonstrate anticancer

1. Introduction

The Cancer Genome Atlas project, the International Cancer Genome Consortium, and other large-scale genomics projects

W. Ngamcherdtrakul, J. Morry, S. Gu, Dr. D. J. Castro, Dr. S. M. Goodyear, T. Sangvanich, M. M. Reda, R. Lee, S. A. Mihelic, B. L. Beckman, Dr. Z. Hu, Prof. J. W. Gray, Prof. W. Yantasee

Department of Biomedical Engineering
Oregon Health and Science University
3303 SW Bond Avenue, Portland, OR 97239, USA
E-mail: grayjo@ohsu.edu; yantasee@ohsu.edu

Dr. D. J. Castro, Prof. W. Yantasee
PDX Pharmaceuticals
24 Independence Avenue, Lake Oswego, OR 97035, USA



DOI: 10.1002/adfm.201404629

efficacy at sites other than the liver (i.e., melanoma). A Phase 1 trial showed that this construct successfully silenced the target gene, RRM2, in tumors of three patients.^[12] However, a subsequent report found that particle instability in kidneys reduced siRNA half-life.^[13] In particular, only 1.4% of the injected siRNA remained in blood at 1 h after injection into nonhuman primates without tumors.^[14] siRNA complexed with tumor penetrating peptides have also shown some efficacy.^[15] Furthermore, a siRNA–peptide complex against PLK1 coupled to a human epidermal growth factor receptor type 2 (HER2) scFv for targeted delivery to HER2⁺ breast cancer was reported to show efficacy in HER2⁺ BT474 xenografts.^[15b]

Inorganic nanoparticles such as gold, mesoporous silica, and iron oxide have been tested as siRNA carriers. These are typically easier to synthesize reproducibly at large scale. Spherical nucleic acid–gold nanoparticle conjugates^[16] have been developed to deliver siRNA against Bcl2Like12 for treating glioblastoma. In vivo protein knockdown ($\approx 40\%$) and antitumor efficacy were achieved in the orthotopically implanted tumor after seven doses administered every other day. Several MSNP-based platforms for siRNA delivery have been tested.^[17] These have exploited passive delivery to areas of tumors that have abnormal molecular and fluid transport dynamics due to abnormal vasculature and lymphatic structure—termed enhanced permeability and retention (EPR).^[18] These MSNPs were coated with cationic polymers including polyethyleneimine (PEI),^[17a,b] PEI–cyclodextrin,^[17c] and PDMAEMA^[17d] for cellular entrance and hence had no cancer cell specificity. Three of the four platforms^[17a,c,d] did not have a steric layer such as polyethylene-glycol (PEG) to shield them from RES recognition.^[19] One PEI-modified MSNP platform without PEG or a targeting agent was employed to deliver siRNA against vascular endothelial growth factor in tumors upon intratumoral injection and shown to inhibit tumor growth.^[17a] Two of the four platforms were loaded with siRNA (siRNA against the M2 isoform of the glycolytic enzyme pyruvate kinase (PKM2)^[17c] or siRNA against polo-like kinase 1 (PLK-1)^[17d] inside the pores, requiring large pore size, and in turn resulting in large particle sizes (80–150 nm as the MSNP core size). While promising, significant antitumor activity in vivo has not been reported for these constructs.^[17c,d] Meng et al.^[17b] reported a PEG–PEI–MSNP platform, but it had no targeting component and showed tumor inhibition only upon combination with a chemotherapy drug (doxorubicin) due to the choice of targeted gene. Overall, MSNP remains attractive as a core material for siRNA delivery in vivo due to its low toxicity, large pore volume,^[20] large surface area, ease of controlling size, and high synthesis scalability.

Following on these reports, we developed a new MSNP construct to deliver siRNA against the oncogenic HER2 gene. We used a small diameter (≈ 50 nm) rigid MSNP as the core. We coated the MSNP core with a PEI polymer to overcome delivery barriers, enable scale-up production, and minimize toxicity compared to PEI–siRNA complexes. PEI was also crosslinked by bioreducible crosslinkers to enhance its buffering capacity. We incorporated a PEG layer to protect the siRNA against blood enzymes, to prevent aggregation of cationic nanoparticles, to enhance blood safety, and to prevent adverse immune response to the nanoparticles. We attached the antibody trastuzumab to the nanoparticle surface to target the particles to cells that

overexpress the HER2 protein and to provide independent therapeutic benefit. Finally, we loaded siRNA on the external surface of the MSNP (but protected under the PEG layer) to allow easy siRNA escape from the endosome prior to degradation by lysosomes.

We chose HER2 as the initial siRNA target because it is a particularly strong and well-validated therapeutic target in breast cancer. Amplification of this gene occurs in 15%–25% of diagnosed breast cancers^[21] and is linked to aggressiveness and poor prognosis.^[22] First line HER2⁺ targeted therapies, trastuzumab and lapatinib, demonstrate significant clinical efficacy, thereby providing validation of HER2 as a therapeutic target. However, up to 70% of patients with advanced disease demonstrate intrinsic or acquired resistance to trastuzumab within one year.^[23] A combination of trastuzumab and lapatinib provided additional benefits to patients, but 50% of patients still did not respond to the treatment.^[24] Combinations with newer therapeutic agents including trastuzumab emtansine, pertuzumab, and neratinib are promising and some will likely become part of the standard of care for HER2⁺ tumors. However, early studies of these agents also show that many tumors still eventually progress on treatment.^[25] Thus, additional therapeutic options are needed. By silencing HER2 in tumors with siRNA in combination with simultaneous trastuzumab delivery, we provide a new strategy that may increase efficacy in tumors that remain dependent on the HER2 pathway, thereby advancing treatment of HER2⁺ breast cancers.

2. Results and Discussion

2.1. Synthesis, Characterization, and Optimization of siRNA–nanoparticles

Our siRNA delivery construct is built around a MSNP core. MSNP size is an important consideration in siRNA–nanoparticle design. Several studies suggest that nanoparticles should be within the size range of 20–200 nm in order to enable EPR-mediated delivery.^[26] We used MSNPs at the smaller end of this size range since we expect that smaller nanoparticles will extravasate best into tumor tissues.^[27] We compared two synthetic methods to produce the MSNP core; one yielded uniform sizes of 34 ± 3 , 47 ± 4 , and 61 ± 7 nm by varying the ratios of two surfactants (designated as S-34, S-47, and S-61, respectively), and the other^[28] yielded particles that were larger and less uniform in size of 87 ± 14 nm (designated as O-87). These results are illustrated in the transmission electron microscope (TEM) images in **Figure 1A–D** and summarized in **Table 1**. We analyzed these MSNPs using Fourier transform Infrared spectroscopy (FT-IR) to make sure there were no remaining surfactants (pore templates) in the NP cores (**Figure S1A**, Supporting Information).

We modified the MSNP core surface as illustrated in **Figure 1E** by adding PEI, PEG, the targeting antibody, and siRNA. We included PEI in these constructs to promote endosomal escape of nucleic acids.^[29] However, the toxicity of PEI is of concern. We attempted to reduce this by adding a PEG layer.^[30] Nanoparticles were further conjugated with

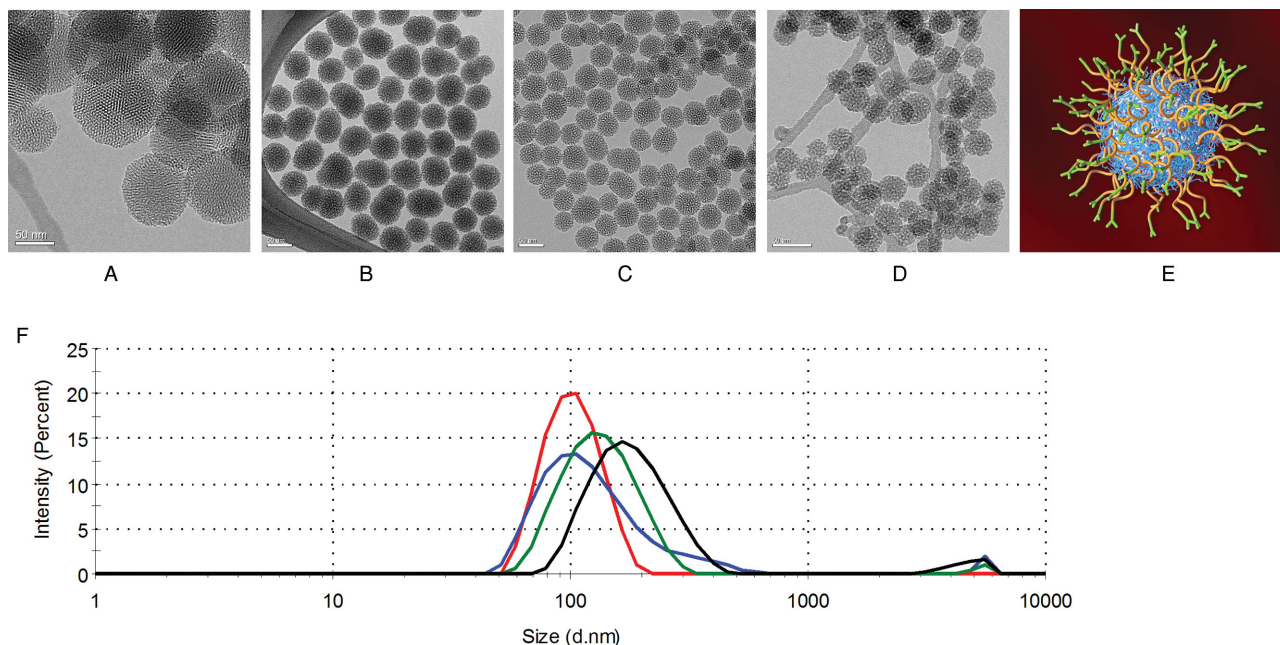


Figure 1. Characterization of mesoporous silica nanoparticle (MSNP) cores and schematic of siRNA–nanoparticles. A–D) TEM images of four batches of mesoporous silica nanoparticle (MSNP) cores: nonuniform-sized MSNP with an average size of 87 nm (O-87, A)), and uniform-sized MSNP with an average size of 61 nm (S-61, B)), 47 nm (S-47, C)), and 34 nm (S-34, D)), respectively (Scale bar = 50 nm). E) Schematic illustration of the nanoparticles with exterior modified layer-by-layer with cationic polymer (crosslinked PEI, blue), PEG (orange), antibody (green), and siRNA (magenta). F) Hydrodynamic size distribution of S-34 (blue), S-47 (red), S-61 (green), and O-87 (black) cores after surface modification as in E) except O-87, of which PEI was coated without crosslinking.

trastuzumab (designated as T) to target cells expressing HER2 and with rituximab targeting CD20 (designated as R) as a negative control. These nanoparticle constructs will be referred to hereafter as T–NP or R–NP, designating trastuzumab-conjugated PEG–PEI–MSNP or rituximab-conjugated PEG–PEI–MSNP, respectively. We employed several siRNAs during the course of our studies including a scrambled siRNA control designated siSCR, a siRNA against luciferase designated siLUC, and a siRNA against HER2 designated siHER2. Their specific sequences are described in the Supporting Information.

The nanoparticles after surface modification had a hydrodynamic size of ≈ 100 nm for the three uniform-sized core materials (S-34, S-47, S-61) and 200 nm for the nonuniform-sized core material (O-87) in phosphate buffered saline (PBS). All materials were also positively charged after the modification due to the cationic PEI. The hydrodynamic sizes and zeta potentials of these materials after surface modification are summarized in Table 1 and hydrodynamic size histograms are shown in Figure 1F. Composition of the optimized nanoparticles (also see Section 2.2) was analyzed by thermogravimetric analysis (TGA) and BCA assay

Table 1. Hydrodynamic size, zeta potential, and silencing efficacy of six different nanoparticles.

Material (MSNP core)	MSNP core size by TEM ^{a)} [nm]	Surface modification ^{b)}	Hydrodynamic size (DLS)		Zeta charge [mV]
			Size ^{c)} [nm]	PDI ^{d)}	
O-87	87 ± 14	T–NP ¹⁰	214 ± 22	0.22	22 ± 0.5
S-61	61 ± 7	T–NP ¹⁰	113 ± 1.0	0.20	18 ± 0.4
		T–NP ^{10C}	131 ± 0.3	0.20	19 ± 3.7
S-47	47 ± 4	T–NP ^{10C}	117 ± 0.5	0.19	25 ± 0.1
		T–NP ^{1.8C}	117 ± 2.4	0.20	19 ± 4.0
S-34	34 ± 3	T–NP ^{10C}	133 ± 4.1	0.37	19 ± 4.0

^{a)}Core size measured in dry state, average size of 50 particles; ^{b)}“10” stands for 10-kDa PEI; “1.8C” and “10C” stand for crosslinked 1.8-kDa and crosslinked 10-kDa PEI, respectively. All PEI-MSNP were then conjugated with PEG, and trastuzumab (T); ^{c)}Average of three measurements; the z-average diameter and polydispersity index (PDI) values were defined according to International Standard on DLS (ISO13321); ^{d)}PDI ranges from 0 to 1; smaller number indicates narrower size distribution; e.g., PDI < 0.05 is considered monodisperse (one size only), while PDI > 0.5 indicates a broad distribution of particle sizes.

Table 2. Composition of T-siRNA-NP (all reported as percent by mass of the whole construct).

Materials	Surface modification	PEI by TGA [%]	PEG by TGA [%]	Antibody by BCA [%]	NP/siRNA mass ratio (fluorescent method)
S-47	T-NP ^{10C}	13.5	18.2	3	Complete at 25 and 50
S-47	T-NP ^{1.8C}	15.9	6.1	3	Complete at 25 and 50

as reported in Figure S1B, Supporting Information, and Table 2.

The siHER2 was selected from 76 potential sequences by measuring the efficacy and specificity with which these siRNAs reduced mRNA levels and growth in four HER2⁺ cell lines and two HER2⁻ cell lines. The best siHER2 from these studies was further confirmed for the efficacy and specificity in 20 additional HER2⁺ cell lines and 2 HER2⁻ cell lines as shown in Figure S2A, Supporting Information. The dose of this siRNA required to inhibit growth by 50% (GI50) was $<5 \times 10^{-9}$ M in 19 of 20 HER2⁺ cell lines including 13 that did not respond to trastuzumab (30 $\mu\text{g mL}^{-1}$) (Figure S2B, Supporting Information).

2.2. Engineering Endo-Lysosomal Vesicle Escape and In Vitro Gene Knockdown by siRNA-Nanoparticles

Internalized nanoparticles ultimately end up in perinuclear lysosomal vesicles. siRNAs must escape from this environment early to be effective since the nucleases and acidic pH in the lysosomal vesicles will destroy the entrapped complexes. Polymers that exhibit high transfection efficiencies, such as PEI,^[31] have buffering capacity in the endo-lysosomal pH range of 5–7 due to presence of unprotonated secondary and tertiary amines. This buffering is thought to increase influx of hydrated protons and chloride ions, thereby causing the vesicles to swell, rupture, and release the siRNAs into

cytosol.^[32] This phenomenon is referred to as the proton sponge effect.

We tested the possibility that endo-lysosomal escape and gene silencing efficacy of our siRNA-nanoparticles could be increased by increasing buffering capacity of the nanoparticles. First, we measured the buffering capacities of nanoparticle platforms with crosslinked 1.8-kDa PEI (T-NP^{1.8C}), crosslinked 10-kDa PEI (T-NP^{10C}), and noncrosslinked 10-kDa PEI (T-NP¹⁰) in 150×10^{-3} M NaCl (see Figure 2A). We found that the nanoparticle platforms had buffering capacity in the order of T-NP^{10C} > T-NP¹⁰ > T-NP^{1.8C}. Thus, the crosslinking of the PEI creates more secondary and tertiary amines yielding greater buffering capacity than primary amines.^[33] We expected that gene silencing efficacy would be in the same order based on the proton sponge mediated siRNA release concept.

We tested this by comparing the gene silencing ability of test siLUC on various nanoparticles (four core sizes, loaded with PEI of 1.8-kDa or 10-kDa, crosslinked or no crosslinked). Specifically, we assessed luciferase silencing at 24 h post exposure of the siLUC-nanoparticles on a breast cancer cell line, MDA-MB-231-H2N-luc, that was genetically modified to overexpress both HER2 and luciferase.^[34] Figure 2B,C shows the luciferase silencing (vs siSCR) of all nanoparticles. Complete siRNA binding was achieved for all materials at NP/siRNA mass ratio of 25 and above (confirmed by no remaining unbound siRNA in the solution phase after the loading step). However, materials with NP/siLUC of 50 offered better gene silencing efficacy

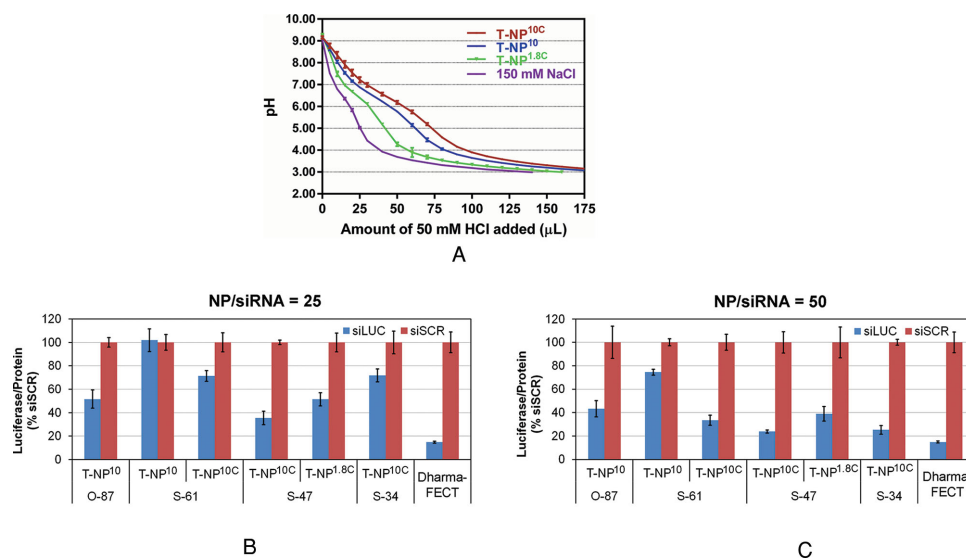


Figure 2. Buffering capacity and luciferase silencing efficacy of nanoparticles. A) Buffering capacity of three nanoparticle platforms with crosslinked 1.8-kDa PEI (T-NP^{1.8C}), and noncrosslinked (T-NP¹⁰) and crosslinked 10-kDa PEI (T-NP^{10C}) measured in NaCl (150×10^{-3} M). B,C) Silencing of luciferase in MDA-MB-231-H2N-luc (high HER2, high luciferase) upon treatment with 30×10^{-9} M siLUC on nanoparticles (NP) at NP/siRNA weight ratio of 25 (B) and 50 (C), measured at 48 h post-transfection (with overnight media change).

(per same dose of siLUC) (Figure 2C) than those with NP/siLUC of 25 (Figure 2B) due to the greater number of nanoparticles to which the cells were exposed. We used the 50 mass ratio throughout this study unless specified otherwise. We found that smaller particles had reduced silencing efficacy compared to larger particles (see S-61 vs O-87, both were modified with 10-kDa PEI, designated as T-NP¹⁰ in Figure 2B). This is likely due to poorer endo-lysosomal escape of the siLUC from the smaller particles. However, large particles are less desirable for tumor delivery using EPR effects. We tested the possibility that the siRNA endosomal release from smaller particles could be enhanced by PEI crosslinking to increase the buffering capacity as shown in Figure 2A. Figure 2B,C shows that the silencing efficacy was indeed improved with crosslinked materials, compared to the noncrosslinked material (see T-NP^{10C} vs T-NP¹⁰, from S-61 core). The highest silencing efficacy (76%) was achieved with the nanoparticles that were developed from S-47 core. This S-47 material also yielded the best size distribution without large aggregates (Figure 1F). The S-47 modified with crosslinked 10-kDa PEI was more effective than that modified with crosslinked 1.8-kDa PEI (76% vs 60% silencing efficacy). Their compositions are reported in Table 2 (see also Figure S1B, Supporting Information, for TGA analysis for PEI and PEG loading characterization). The S-47 core material with crosslinked PEI was used for all subsequent experiments.

2.3. Protection of siRNA against Blood Enzymatic Degradation

We assessed the ability of MSNP constructs (T-siHER2-NP^{1.8C} vs T-siHER2-NP^{10C}) to protect siHER2 from degradation by blood enzymes by measuring the amount of siHER2 remaining after incubation of siHER2-nanoparticles for 0–48 h in human serum (50% in PBS) at 37 °C. We compared these results to those obtained for free siHER2 without nanoparticles. Figure 3A shows the amount of intact siHER2 that survived enzymatic degradation as measured by gel electrophoresis. The corresponding siHER2 quantification based on the band intensity and location is shown in Figure 3B. Without the nanoparticles, naked siHER2 was degraded within 0.5 h (observed as bands shifted toward lower molecular weight), and its half-life

was about 1 h, in agreement with previous reports for other siRNAs.^[35] T-siHER2-NP^{1.8C} fully protected siHER2 up to 8 h, while T-siHER2-NP^{10C} fully protected siHER2 up to 24 h. The siRNA on both of our nanoparticle platforms appeared to experience much less degradation than siRNA on the cyclodextrin-based nanoparticles which have already shown clinical anti-tumor efficacy.^[12b] Those cyclodextrin-protected siRNAs were reported to experience 50% degradation within 12 h, and 70% within 24 h under 50% serum conditions.^[36]

2.4. Importance of PEG

The higher siRNA protection for T-siHER2-NP^{10C} compared to T-siHER2-NP^{1.8C} is likely due to the increased PEG content for the higher-molecular-weight PEI of T-siHER2-NP^{10C}. The PEG contents of T-siHER2-NP^{10C} and T-siHER2-NP^{1.8C} were 18.2% and 6.1%, respectively (Table 2). Higher PEG content is expected for T-siHER2-NP^{10C} since it contains more reactive amine groups for PEG binding than T-siHER2-NP^{1.8C}. PEG is known to provide a steric blocking effect^[37] that reduces enzymatic degradation of siRNA.^[38] It also reduces binding of blood proteins to the nanoparticles.^[37b] We found in a separate experiment (Figure S3A, Supporting Information) that siRNA on PEI-MSNP without PEG degraded faster than naked siRNA since positively charged PEI recruited more negatively charged siRNA degrading enzymes. In addition, we found significant aggregation of nanoparticles without PEG upon siRNA loading (Figure S3B, Supporting Information). The PEG layer also improved blood compatibility and reduced immune response as described later in the paper.

2.5. Cellular Uptake of the siRNA-Nanoparticles

Cellular uptake relies on HER2 antibody (trastuzumab) conjugated on the nanoparticles, which was found to be optimal at 3% by mass of trastuzumab per nanoparticles as shown in Figure S4, Supporting Information. This 3% loading was used throughout the paper. Without trastuzumab (Figure S4, Supporting Information), the nanoparticles could be taken up by

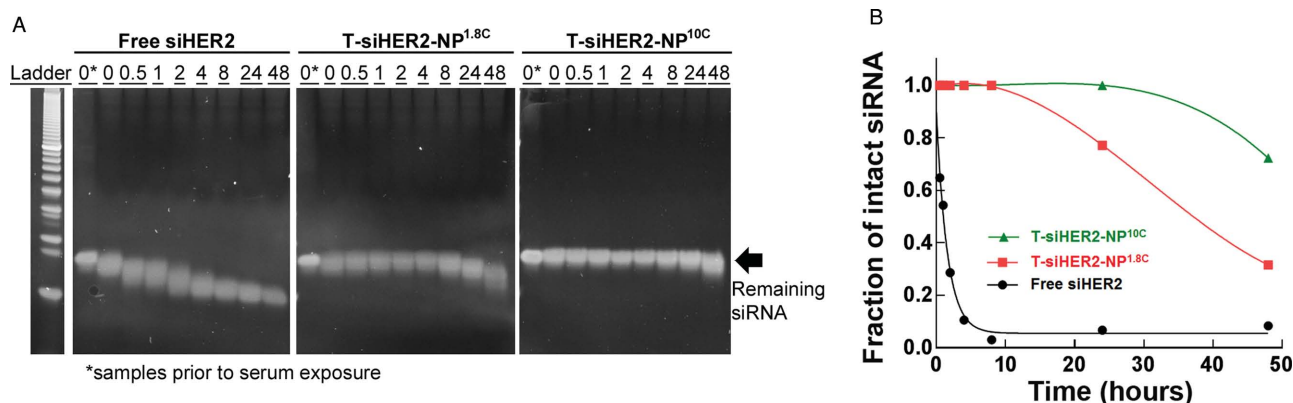


Figure 3. siRNA protection from serum degradation. A) Residual siRNA against HER2 (siHER2) band after contact with 50% human serum after specified periods of time; conducted with free siHER2, or siHER2 loaded on two nanoparticle platforms with crosslinked 1.8-kDa (T-siHER2-NP^{1.8C}) and crosslinked 10-kDa PEI (T-siHER2-NP^{10C}), all at 37 °C with shaking, and B) the corresponding siHER2 quantification using ImageJ software.

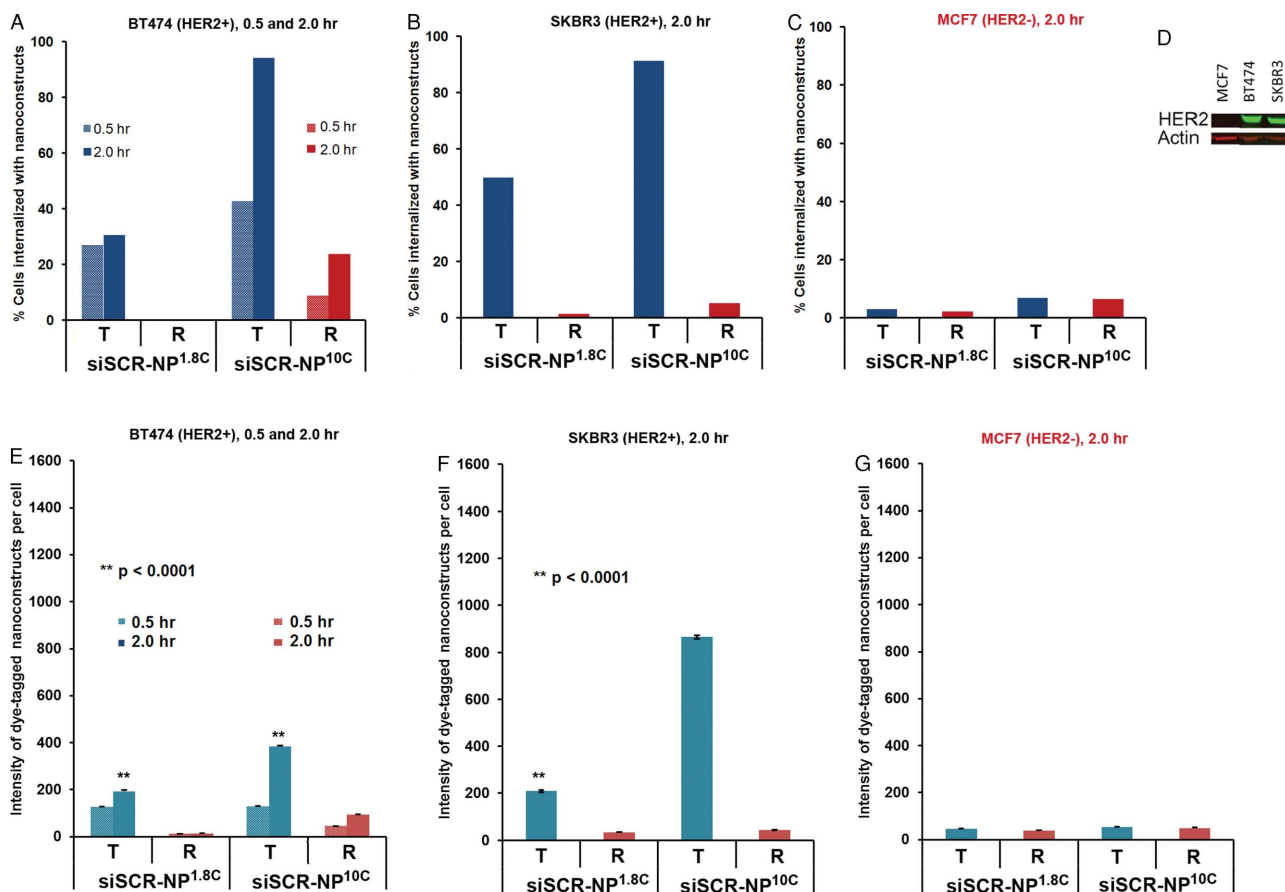


Figure 4. Cellular uptake of siRNA–nanoparticles. Percentage of A) BT474 (HER2⁺), B) SKBR3 (HER2⁺) breast cancer cells, and C) MCF7 (HER2⁻) breast cancer cells, that were internalized with fluorescent dye-tagged scrambled siRNA (siSCR)–nanoparticles having either crosslinked 1.8-kDa (NP^{1.8C}) or crosslinked 10-kDa PEI (NP^{10C}), and conjugated with either trastuzumab (T) or rituximab (R), D) western blot confirming HER2 content of these three cell lines, and E–G) the corresponding intensity (per cell) of dye-tagged siSCR–nanoparticles internalized into the cells. Data were presented as mean \pm SEM. All were performed with 1×10^6 cells and 100 μ g of nanoparticles in 0.3 mL of cell culture media and exposure time of 0.5 or 2 h. Also see histogram in Figure S5, Supporting Information.

cells due to their positive charge, which is not specific to targeted cells only. Next, we assessed the specificity with which trastuzumab-targeted siRNAs were taken up by cells that overexpress the HER2 protein by measuring the uptake of nanoparticles carrying a scrambled siRNA and coupled with trastuzumab (designated hereafter as T–siSCR–NP^{1.8C} and T–siSCR–NP^{10C}) and with rituximab targeting CD20 (designated as R–siSCR–NP^{1.8C} and R–siSCR–NP^{10C}). We measured cellular uptake of T–siSCR–NP^{10C} and T–siSCR–NP^{1.8C} in HER2⁺ breast cancer cells, BT474 and SKBR3, and the HER2⁻ cell line MCF-7 at 0.5 or 2.0 h post exposure to the nanoparticles. The siSCR was tagged with the fluorescent reporter, Alexa 488, for these experiments to enable quantitative analysis of siSCR uptake. R–siSCR–NP^{10C} and R–siSCR–NP^{1.8C} nanoparticles served as a negative control since BT474, SKBR3, and MCF-7 cells weakly express CD20. We measured the amount of Alexa 488-tagged siSCR in the interior of individual cells using flow cytometry after quenching fluorescence from Alexa 488-tagged siSCR on the external cell membrane using Trypan blue. **Figure 4A–C** shows that T–siSCR–NP^{10C} were taken up effectively (>90%) into HER2⁺ cells (BT474 and SKBR3), but not HER2⁻ cells (MCF7) and that uptake increased by extending

the exposure time from 0.5 to 2 h. Furthermore, uptake of T–siSCR–NP^{10C} was greater than T–siSCR–NP^{1.8C}. In addition, R–siSCR–NP^{10C} and R–siSCR–NP^{1.8C} nanoparticles were not taken up efficiently by any of the cell lines. **Figure 4D** illustrates HER2 protein expression in the three cell lines being evaluated. **Figure 4E–G** shows the average intensity of Alexa 488-tagged siSCR signal per cell and the same trend can be observed. Fluorescence distributions of Alexa 488-siSCR uptake are reported in **Figure S5**, Supporting Information. This confirms that nanoparticles enter cells primarily by a HER2-receptor-mediated endocytosis mechanism and not by adsorptive endocytosis of positively charged particles as reported for PEI–MSNP.^[39]

2.6. HER2 Knockdown Efficacy and Therapeutic Effects

We assessed the efficiency of T–siHER2–NP^{10C} and T–siHER2–NP^{1.8C} in inhibiting HER2 mRNA levels and HER2 protein expression in the HER2⁺ breast cancer cell lines, BT474, SKBR3, and HCC1954. We used quantitative immunofluorescent imaging (IF) to assess HER2 protein levels (**Figure 5A**), the Quantigene RNA assay for HER2 mRNA level (**Figure 5B**),

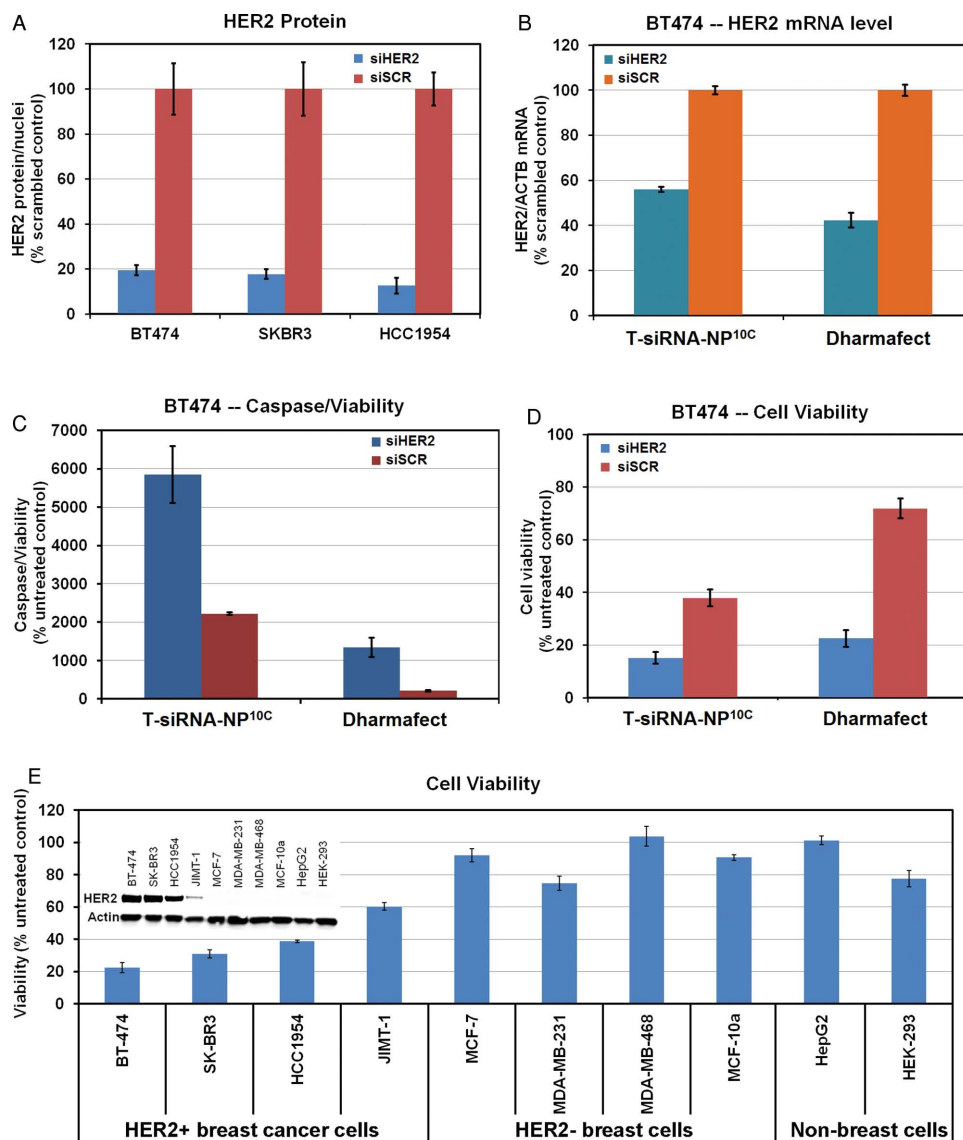


Figure 5. HER2 knockdown by siHER2–nanoparticles and therapeutic responses. A) HER2 expression of three HER2⁺ breast cancer cells at 72 h post-treatment with siHER2 or siSCR (60×10^{-9} M) on T-NP^{10C}. B) HER2 mRNA level (48 h), C) apoptotic activity (four days), and D) cell viability (four days) of BT474 cells treated the same way as (A). E) Cell viability after treatment with T–siHER2–NP^{10C} for four days in various cell lines. All cells exposed to siRNA–nanoparticles overnight and media changed. Inset of (E) shows HER2 levels of all cells tested.

cleaved Caspase 3 and 7 assay for apoptotic markers (Figure 5C), and cellular ATP level assay for cell viability (Figure 5D,E). Figure 5A shows that T–siHER2–NP^{10C} reduced HER2 levels by 81%–93% compared to T–siSCR–NP^{10C}. Figure S6A, Supporting Information, shows that the T–siHER2–NP^{10C} were more effective than T–siHER2–NP^{1.8C} at equivalent siRNA dose. Also, Figure S6B, Supporting Information, shows that doubling the dose of T–siHER2–NP^{1.8C} did reduce HER2 protein levels by 79%–83% in SKBR3 and HCC1954 but even that was not effective in BT474 cells. Overall, T–siHER2–NP^{10C} demonstrated better anti-HER2 efficacy than T–siHER2–NP^{1.8C}. Encouragingly, the T–siHER2–NP^{10C} outperformed siHER2 with DharmafECT in all cell lines as shown in Figure S6C, Supporting Information.

Quantitative interpretation of these results is complicated by the fact that treatment with T–siSCR–NP^{10C} also reduced

HER2 levels and killed HER2⁺ breast cancer cells (Figure S6D, Supporting Information). We attribute this to the high levels of trastuzumab on the nanoparticles (3% by weight) since trastuzumab by itself is known to impact HER2 expression and cell viability independent of the siHER2.^[40] Figure S6D, Supporting Information, for example, shows that HER2 levels in BT474 were reduced by 41% with T–siSCR–NP^{10C} and by 87% with the T–siHER2–NP^{10C} compared to untreated controls. Likewise, Figure 5D shows that cell viability was reduced 59% by T–siSCR–NP^{10C} and 86% by T–siHER2–NP^{10C}. Hence, to evaluate the effect of siRNA, we compared results to the siSCR control instead of the untreated control. We also assessed T–siHER2–NP^{10C} induced changes in HER2 mRNA levels in BT474 at 48 h post-treatment. Figure 5B shows a 44% reduction in HER2 mRNA relative to siSCR control. This compares with

a 58% reduction using DharmaFECT (positive control). These results may be affected by the high cell death induced by the T-siHER2-NP^{10C} since cells that are most strongly affected will be preferentially lost. We gained some insight into this by comparing knockdown efficiency in cells that are more resistant to trastuzumab, such as JIMT1 and HCC1954. In Figure S7, Supporting Information, for example, we found that the mRNA reduction induced by T-siHER2-NP^{10C} and DharmaFECT were more comparable; 69% versus 72% in JIMT1 cells and 57% versus 63% in HCC1954 cells.

Figure 5C shows that apoptotic activity was threefold greater after treatment with T-siHER2-NP^{10C} than with T-siSCR-NP^{10C}, consistent with the reduced cell viability in Figure 5D. We also measured cell viability after treatment with T-siHER2-NP^{10C} in a panel of HER2⁺ cells and HER2⁻ cells. Figure 5E shows that treatment with T-siHER2-NP^{10C} reduced viability more strongly in HER2⁺ breast cancer cells (BT474, SKBR3, HCC1954, and JIMT-1) than in HER2⁻ breast cancer cells (MCF-7, MDA-MB-231, MDA-MB-468), HER2⁻ breast epithelial cells (MCF-10a), HER2⁻ human liver carcinoma cells (HepG2), and HER2⁻ human embryonic kidney cells (HEK-293). The HER2 expression levels of these cells are included as an inset of Figure 5E.

2.7. Impact of T-siHER2-NP^{10C} on Trastuzumab-Resistant Cells

We assessed the efficacy of T-siHER2-NP^{10C} in the intrinsically trastuzumab-resistant HER2⁺ cell lines, HCC1954 and JIMT1 (Figure S2B, Supporting Information), in the HER2⁺ cell line, BT474, that responds to trastuzumab and lapatinib, and in BT474-R, a derivative cell line that was made lapatinib-resistant by long-term treatment with 1×10^{-6} M lapatinib. Figure 6A

shows that the BT474-R cells were also less responsive to trastuzumab compared to parental BT474. However, Figure 6B shows that both cell lines were responsive to T-siHER2-NP^{10C} compared to the T-siSCR-NP^{10C} control. This suggests a similar response to siRNA treatment in both cell lines. Meanwhile, Figure 6C shows that T-siHER2-NP^{10C} reduced the viability of BT474 and BT474-R to 26.9% and 38.3% of the untreated control, respectively. We attribute the reduced efficacy (in terms of cell death compared to the untreated control) in BT474-R to the fact that trastuzumab on the nanoparticles does not elicit any therapeutic effect on BT474-R.

2.8. Blood Compatibility

It is important that nanoparticle constructs intended for use systemically in vivo do not cause hemolysis, thrombogenesis, and platelet aggregation. We assessed these endpoints for T-siHER2-NP^{1.8C} and T-siHER2-NP^{10C}, and compared the results to those for the FDA-approved nanoparticle products: Abraxane (Paclitaxel-albumin nanoparticles) and Feraheme (iron oxide nanoparticles used as a MRI contrast agent). Nanoparticles were tested at 1× and 5× of the intended human blood level. Figure S8A, Supporting Information, shows that T-siHER2-NP^{1.8C} and T-siHER2-NP^{10C} did not cause hemolysis of red blood cells at either dose, while complete blood lysis was achieved with Triton-X (0.025%), the positive control. Figure S8B, Supporting Information, shows that these nanoparticles also did not affect the coagulation time of platelet poor plasma since all took about 37 s, while Feraheme prolonged the coagulation time, in agreement with its known side effects related to abnormal clotting.^[41] Figure S8C, Supporting Information, shows that our nanoparticles and Abraxane did not

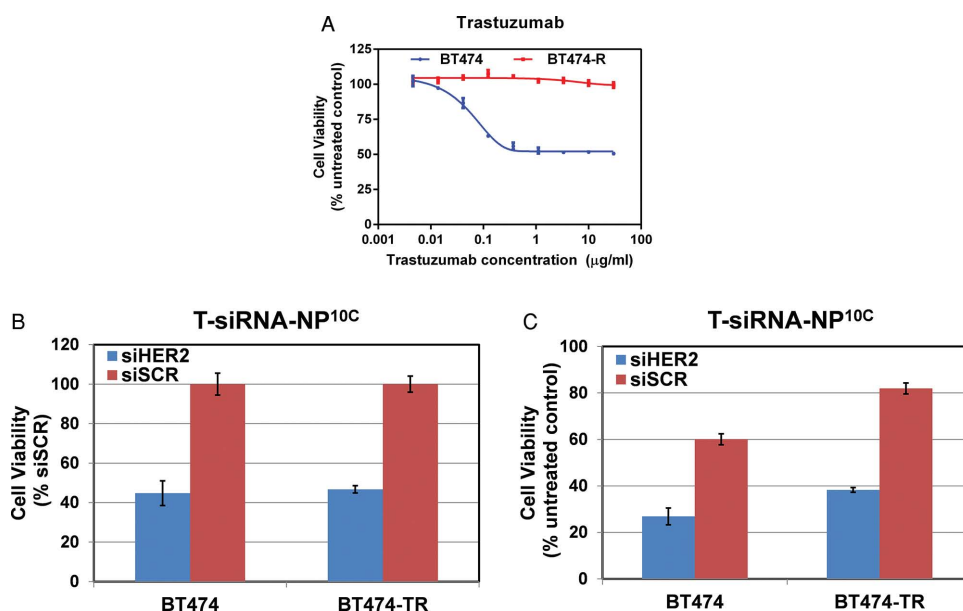


Figure 6. In vitro evaluation of siHER2-nanoparticles on HER2 silencing and ability to overcome trastuzumab resistance. A) Trastuzumab dose response (as five-day cell viability) of BT474 and BT474-R (trastuzumab and lapatinib-resistant cell line derived from prolonged treatment of BT474 cells with lapatinib (1×10^{-6} M)). B,C) BT474 and BT474-R were treated with one dose of T-NP^{10C} loaded with siHER2 or siSCR (60×10^{-9} M siRNA) and cell viability was monitored at five days post-treatment and reported as a percentage of B) siSCR control or C) untreated control.

trigger platelet aggregation while a collagen-related peptide used as a positive control triggered aggregation immediately.

2.9. Immune Response

Induction of an adverse immune response is one of the major causes of failure of drug candidates during preclinical and clinical studies. Nanoparticles may elicit an inflammatory response in immune cells via toll-like receptor activation. We evaluated the effect of T-siHER2-NP^{1.8C} and T-siHER2-NP^{10C} on immune response by treating peripheral blood mononuclear cells (PBMCs) isolated from human blood with these nanoparticles. We measured induction of the cytokines IL-1 β , IL-6, IFN- α , and TNF- α because their production is associated with Toll-like receptor activation on the surface of the cell membrane and on the endosomes.^[42] PBMCs have been reported to respond to siRNA transfection with a sequence-specific TLR 7/8 dependent induction of IFN- α and TNF- α .^[43] We used the TLR7/8 agonist (R848) as a direct positive control since TLR7 and TLR8 are located within the endosomes^[44] where nanoparticles and siRNA are expected to reside. We compared results for our nanoparticles to those obtained for the FDA-approved nanoparticle-based drugs, Abraxane and Feraheme. **Figure 7** shows that neither

T-siHER2-NP^{1.8C} nor T-siHER2-NP^{10C} increased the levels of IL-6 and TNF- α at either the 1 \times or 5 \times level, while Abraxane significantly increased both cytokines at the 5 \times level. Both nanoparticles increased the levels of IFN- α and IL-1 β somewhat, but not to the extent observed for Abraxane for IL-1 β and Feraheme for IFN- α . The immune response was not significantly different for nanoparticles with or without siRNA, suggesting that the response was not siRNA specific. Finally, the PBMC immunological response to T-siHER2-NP^{10C} was not worse than T-siHER2-NP^{1.8C}. This may be because the higher PEG content of T-siHER2-NP^{10C} (Table 2) compensates for its higher charge of higher-molecular-weight PEI. We tested our nanoparticles for lipopolysaccharides or LPS, produced by gram-negative bacterial contamination since this might also trigger an adverse immune response. About 35% of clinically relevant nanoparticles have been found to carry this contaminant.^[45] Figure S9, Supporting Information, shows that T-siHER2-NP^{1.8C} and T-siHER2-NP^{10C} were not contaminated.

2.10. In Vivo HER2 Silencing Efficacy and Tumor Growth Inhibition in an Orthotopic Mouse Tumor Model

We chose the T-siHER2-NP^{10C} (with S-47 MSNP core) over T-siHER2-NP^{1.8C} because it yielded higher siHER2 protection,

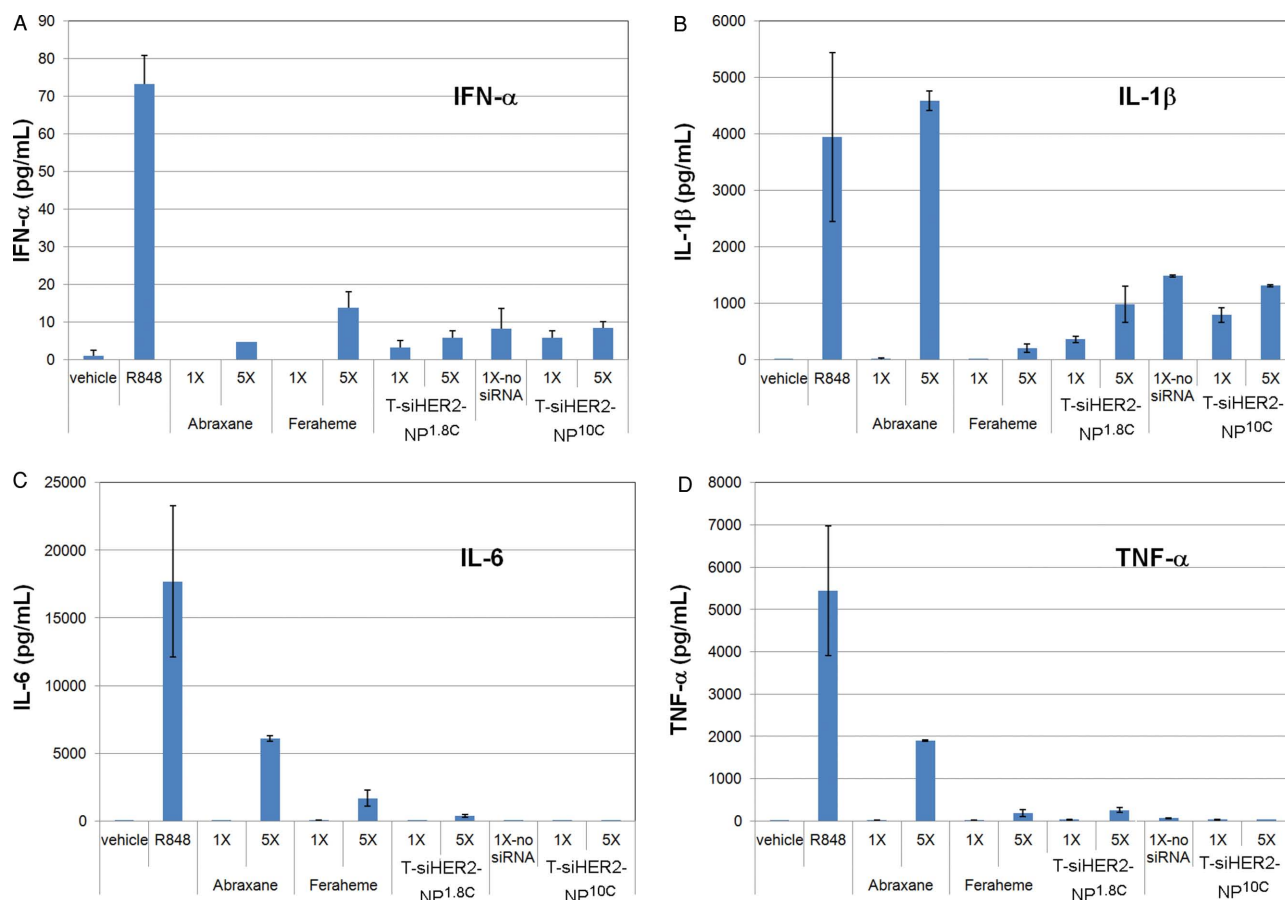


Figure 7. Cytokine induction in PBMCs. 24-h exposure with various nanoparticles, T-siHER2-NP^{1.8C}, T-NP^{10C} (no-siRNA), T-siHER2-NP^{10C}, Abraxane, and Feraheme. 1 \times = estimated human blood levels of the materials (i.e., 94 $\mu\text{g mL}^{-1}$ for Abraxane, 102 $\mu\text{g mL}^{-1}$ for Feraheme, and 70 $\mu\text{g mL}^{-1}$ for the two nanoparticles), 5 \times = fivefold of such levels, Vehicle = PBS, R848 = TLR7/8 agonist (10×10^{-6} M).

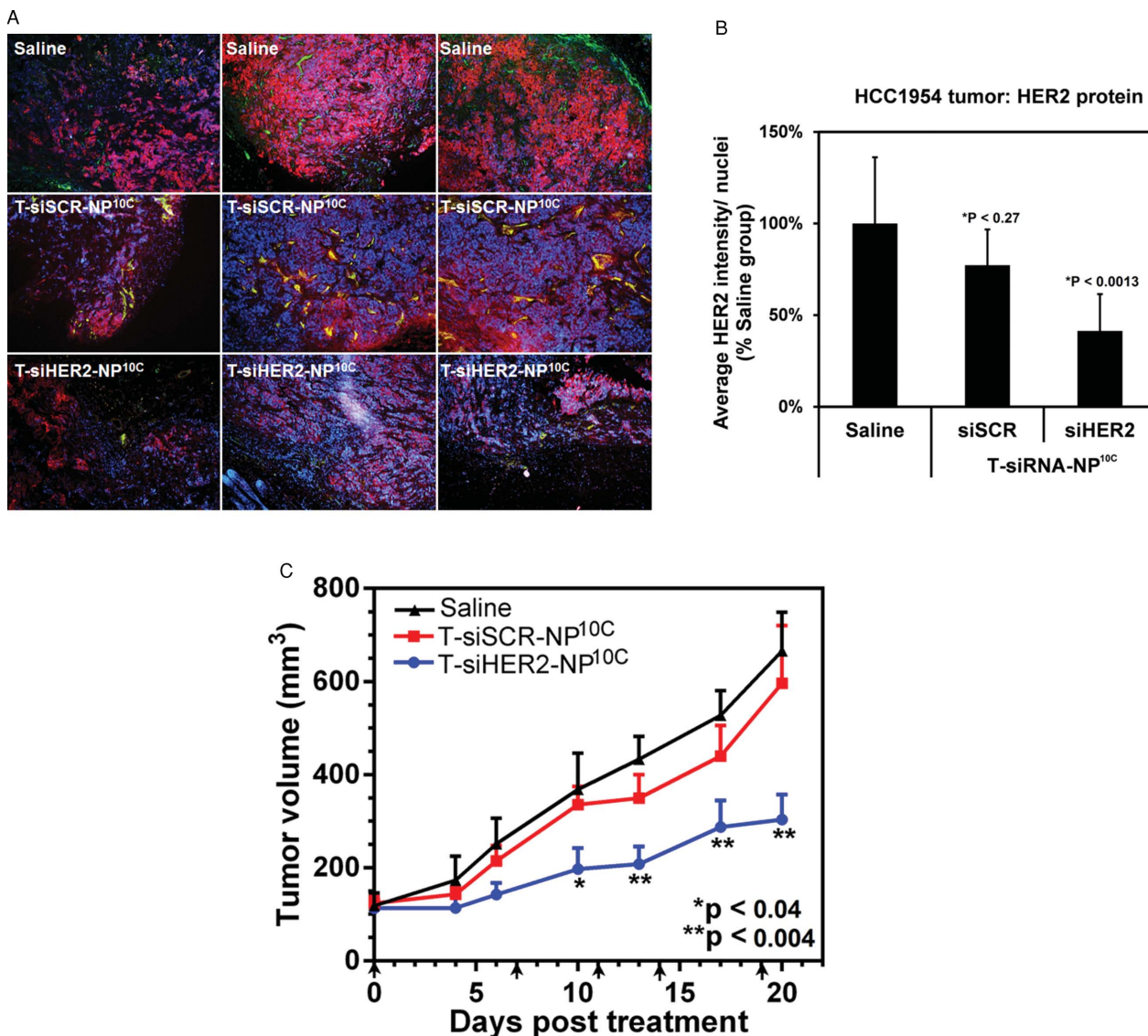


Figure 8. In vivo HER2 reduction and growth inhibition of orthotopic HCC1954 tumors. A) Representative immunofluorescent images of tumor tissues collected from mice ($n = 4/\text{group}$) at four days post i.v. injection with one dose of T-NP^{10C} loaded with siHER2 or siSCR (1.25 mg siRNA kg⁻¹, NP/siRNA of 50) or PBS control. B) Quantitative HER2 levels of the tissues (means \pm SD). Images were analyzed by CellProfiler; red = HER2 protein; green = CD31 endothelial marker; blue = DAPI staining cell nuclei. C) Tumor growth in mice bearing orthotopic HCC1954 tumor xenografts ($n = 5/\text{group}$) receiving the same treatments as (A) but multiple doses (days of injection are indicated by arrows). Tumor volumes are presented as means \pm SEM. Specified p -values are against the saline control.

better cellular uptake, and higher gene knockdown and cell killing efficacy, without greater toxicity. Accordingly, we evaluated T-siHER2-NP^{10C} for in vivo gene knockdown efficacy in HCC1954 xenografts grown orthotopically in mammary fat pads. Tumors were allowed to grow to 250 mm³ before treatment ($n = 4$ per group). We administered T-siHER2-NP^{10C} and T-siSCR-NP^{10C} as a single intravenous tail vein injection in order to deliver 1.25 mg siRNA kg⁻¹ body weight. Tumors were harvested at four days post-injection and analyzed. **Figure 8A,B** shows the HER2 protein levels in the HCC1954 tumors were reduced by 58.6% compared to saline control ($p < 0.0013$) and by 46.5% compared to treatment with the T-siSCR-NP^{10C} control ($p < 0.015$). It should be noted that 22.7% ($p = 0.27$ vs

saline control) of the HER2 reduction in the siSCR control is likely due to trastuzumab on the nanoparticles. Similar results were obtained with orthotopic JIMT-1 tumor model as shown in Figure S10, Supporting Information, but to a lesser extent (e.g., 38.2% HER2 reduction versus saline control ($p < 0.0012$)). This is perhaps due to lower level of HER2 expression in JIMT1 compared to HCC1954, resulting in reduced nanoparticle delivery and correspondingly reduced knockdown efficacy.

We assessed the ability of T-siHER2-NP^{10C} (with S-47 MSNP core) to inhibit tumor growth in the same HCC1954 mouse model. Tumors were allowed to grow to ≈ 100 –150 mm³ in size prior to group randomization ($n = 5$ per group). Figure 8C shows that five intravenous tail vein injections of 1.25 mg siRNA kg⁻¹

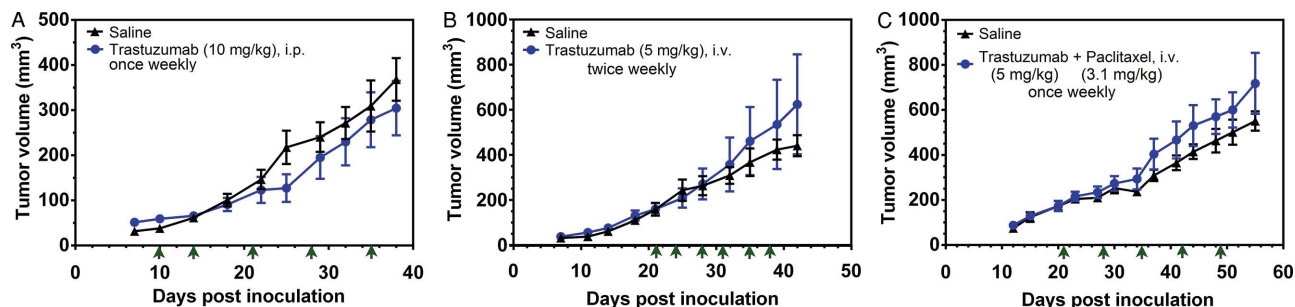


Figure 9. Drug resistance in HCC1954 in vivo. Tumor growth in mice bearing orthotopic HCC1954 tumor xenografts. A) Mice ($n = 7$ /group) were injected intraperitoneally with trastuzumab (10 mg kg^{-1}) or saline. B) Mice ($n = 5$ /group) were injected via tail vein with trastuzumab (5 mg kg^{-1}). C) Mice ($n = 9$ /group) were injected via tail vein with trastuzumab (5 mg kg^{-1}) and paclitaxel (3.1 mg kg^{-1}). Arrows indicate days of injection. Tumor volumes are presented as means \pm SEM.

over a period of three weeks significantly inhibited tumor growth, while T-siSCR-NP^{10C} produced little effect. This response is noteworthy since HCC1954 has been established as resistant to cisplatin,^[46] trastuzumab,^[47] and pertuzumab^[48] in vitro and/or in mice. We confirmed its resistance in vivo to trastuzumab (Figure 9A,B) and trastuzumab and paclitaxel combination (Figure 9C). We also found that T-siRNA-NP¹⁰ (with O-87 core) inhibited ectopic HCC1954 xenograft growth (Figure S11A, Supporting Information), while the siSCR control did not. In orthotopic tumors, however, T-siHER2-NP^{10C} (with S-47 MSNP core) showed better efficacy than the larger particles, even at half the dose of siRNA (i.e., $1.25 \text{ mg siRNA kg}^{-1}$ in Figure 8C vs $2.5 \text{ mg siRNA kg}^{-1}$ in Figure S11B, Supporting Information).

2.11. Reproducibility of Nanoparticle Synthesis

It is often difficult to achieve high batch-to-batch reproducibility during nanoparticle synthesis. We achieved manufacturing control of particle size and surface modification by combining inorganic and polymeric materials. Our sol-gel chemistry affords high batch-to-batch reproducibility of the MSNP core with 2.4% relative standard deviation (RSD) of particle sizes from six batches (Figure S12A,B, Supporting Information). The layer-by-layer surface modification was also reproducible as shown in Figure S12A,C, Supporting Information. Washing after each of the loading steps facilitates impurity removal. This is difficult to accomplish with one-pot synthesis methods. Based on these results, we anticipate that it will be straightforward to scale the sol-gel chemistry and the layer-by-layer modification manufacturing processes to the level needed for clinical studies.

3. Conclusion

We have produced a new generation siRNA in vivo delivery construct comprised of a MSNP core coated with PEI polymer to enhance delivery, a PEG layer to protect the siRNA and attached to an antibody for targeted delivery. We have demonstrated that our most effective construct, T-siHER2-NP^{10C} (with S-47 core) was effectively taken up by HER2⁺ cells in a specific manner via antibody-receptor interaction and effectively silenced HER2 expression in vitro and in vivo. It did not appear to elicit

unacceptable immune responses. This construct also produced excellent HER2 knockdown and growth inhibition of drug-resistant HER2⁺ tumor xenografts grown orthotopically. Manufacturing of the construct is straightforward, reproducible, and can be scaled to the level needed for clinical use.

HER2 oncogene/protein was chosen as the initial therapeutic target for siRNA (siHER2). Our data show that cancer resistant to current HER2 targeted therapies (e.g., trastuzumab and lapatinib) still responds well to siHER2 treatment. In addition to serving as a homing target, HER2 Ab (trastuzumab) also displays therapeutic effect, when conjugated on our nanoparticles. This provides a strong motivation to have both HER2 Ab and siHER2 on the same nanoparticle. With regard to the potential self-defeating issue that HER2 proteins might be decreased in the treated cells, rendering the targeting by HER2 Ab ineffective, we have two hypotheses: (1) not all cells within the tumors will receive T-siHER2-NP at once and hence some cells still overexpress HER2 for HER2 Ab-assisted delivery in subsequent doses, and (2) cells that receive sufficient T-siHER2-NP will undergo apoptosis (hence no longer needing T-siHER2-NP delivery) and the surviving cells will replenish HER2 proteins for HER2 Ab-assisted delivery in subsequent doses. We found that cells that survived long-term continuous treatment with siHER2, due to either not receiving sufficient siHER2 or not having siHER2 delivery at all, could replenish their HER2 level once relieved of siHER2 treatment to the same level with naïve cells. This indicates that they can still be the target for delivery by HER2 Ab. Our data also showed that long-term siHER2 treated cells remained sensitive to siHER2 treatment (same percent cell death as the parental or naïve cells). These findings will be reported in due course.

To move this technology forward to clinics, in addition to HER2, we are also actively working on finding other gene targets amenable to HER2⁺ breast cancer and other cancer types. We expect that this construct can be adapted to silence any gene deemed important in cancer growth. The siRNA-nanoparticle has the potential to impart both delivery specificity and therapeutic specificity via the RNAi mechanism, potentially providing a greater therapeutic index than conventional chemotherapeutics or small molecule inhibitors. In our platform, siRNA loading was accomplished last using a simple and quick mixing method. The loading employs electrostatic interaction, relying on negatively charged phosphodiester siRNA backbone. Therefore, the loading efficiency is independent of

siRNA sequences. Our platform thus affords loading of different siRNAs or a cocktail of siRNAs without difficulty. In addition, since siRNA is loaded outside, our platform permits loading of drugs or imaging agents inside the pores, if needed. Co-delivery of drugs or imaging agents with siRNA has been investigated in our lab, but is outside the scope of this paper.

4. Experimental Section

Materials, siRNA, and Cell Lines: Detailed information on reagents and siRNA used is provided in the Supporting Information. Human breast cancer cell lines (BT474, JIMT1, SKBR3, HCC1954, MCF7, MDAMB231, and MDAMB468), breast epithelial cells (MCF-10a), human liver carcinoma (HepG2), and human embryonic kidney cells (HEK-293) were obtained from American Type Culture Collection. MDAMB231-H2N-luc was obtained as a gift from Prof. Robert Kerbel (University of Toronto, Canada). Cell media recipe for each cell line and siRNA sequence description are provided in the Supporting Information.

Synthesis and Characterization of Nanoparticles: The sol-gel synthesis of MSNPs was modified from previous reports.^[49] For 47-nm NP (S-47), CTAC (0.15 M) and TEA (350 μ L) were mixed in water (125 mL) at 95 °C. Then, TEOS (3 mL) was added and the mixture was stirred for 1 h. Afterward, the pellets were recovered from suspension by centrifugation, washed with a copious amount of ethanol, and dried overnight. The particles were then resuspended and refluxed in acidic methanol (0.6 M HCl in methanol) overnight to remove CTAC and TEA. Bare MSNPs were then washed with ethanol and dried in a desiccator. TEA was also varied from 200 to 450 μ L to achieve the MSNP sizes of 60 and 30 nm, respectively. MSNP (dry) size was measured with TEM (Phillips/FEI CM120/Biotwin TEM, Hillsboro, OR) and hydrodynamic size with Zetasizer (ZS-90/Malvern, Westborough, MA). Nonuniform MSNPs (O-87) were synthesized by base-catalyzed synthesis. CTAB (6 \times 10⁻³ M) was dissolved in aqueous solution of pH 11.0 (240 mL, adjusted by 2 M NaOH). When the temperature stabilized at 80 °C, TEOS (2.5 mL) was added. The reaction continued for 2 h and particles were processed for surfactant removal in the same fashion as explained above. Coating of PEI on the exterior of MSNP was carried out in ethanol by shaking MSNP (10 mg) and PEI (2.5 mg) in ethanol solution for 3 h at room temperature (RT). Next, PEI-MSNPs were crosslinked with DSP crosslinker (0.2 mg) for 40 min. The particles were pelleted down, washed, and resuspended in PBS (pH 7.2). For PEG loading, mal-PEG-5 kDa-NHS (50 mg) was conjugated to the primary amine of MSNP-PEI (10 mg) in the PBS buffer under shaking (20 h, RT, 300 rpm). The PEI and PEG loading were analyzed by TGA (Q50/TA Instruments, New Castle, DE). Antibody conjugation of MSNP-PEI-PEG utilized a thiol-maleimide reaction modified from literature.^[50] First, antibody (trastuzumab (T) or rituximab (R)) was thiolated with Traut's reagent in PBS (pH 8.0) by 50-fold molar excess of Traut's reagent for 2 h and then purified by Zeba spin column – MW-40 000 (Thermo Fisher Scientific, Waltham, MA). Thiolated antibody was mixed with MSNP-PEI-PEG at varied mass ratio from 0:1 to 1:1. The reaction was completed overnight at 4 °C under shaking conditions (300 rpm). The material was pelleted down, resuspended in PBS, and washed with copious amount of PBS. Pierce BCA protein assay kit (Thermo Fisher Scientific, Waltham, MA) was used to quantify the antibody loading of the nanoparticles. Finally, the loading of siRNA was achieved by mixing MSNP-PEI-PEG-T (designated as T-NP) and siRNA (at nanoparticle/siRNA mass ratio of 25 or 50) in PBS solution (1 h, room temperature, 200 rpm shaking). The loading of siRNA was monitored by the fluorescent dyes tagged on siRNA.

Luciferase Knockdown Efficacy: The MDAMB231-H2N-luc cell line (overexpressing luciferase and HER2) was used for initial gene silencing efficacy assessment of the nanoparticles loaded with siRNA against luciferase (siLUC). Cells were plated at 3000 cells/well in a 96-well plate, maintained in corresponding cell media, as reported in the Supporting Information. One day after seeding, cells were treated with siRNA-

nanoparticles. The nanoparticles were loaded with siRNA at NP/siRNA ratio of 25 or 50 by mass. They were applied to each well at a fixed dose of 30 \times 10⁻⁹ M siRNA. The commercially available transfection agent, DharmaFECT (GE Dharmacon, Lafayette, CO), with the same siRNA dose (following manufacturer's recommended protocol) served as a positive control. After overnight incubation (\approx 20 h), cells were washed once and replenished with complete media. At 48 h post-treatment, cells were lysed and analyzed for luciferase activity by Luciferase Glow Assay Kit (Thermo Fisher Scientific, Waltham, MA) and protein concentration by BCA protein assay kit (Thermo Fisher Scientific, Waltham, MA), following manufacturer's protocols. Luciferase activity of the lysate was normalized with the corresponding protein concentration in the same well and reported as a percentage of the untreated control. All treatments were performed in quadruplicate.

Buffering Capacity Measurement: Nanoparticles were suspended at 0.2 mg mL⁻¹ in NaCl (150 \times 10⁻³ M, pH 9—pH adjusted with 0.05 M NaOH). Upon stabilization at pH 9.0, HCl (5 μ L, 0.05 M) was added and solution was continuously stirred. When reaching steady state, the pH was recorded and the acid was added again. The process was repeated until the pH plateaued at around 3.0. The solution pH was then reported as a function of the amount of acid added.

Serum Enzymatic Protection Assay: siRNA-nanoparticles were incubated with human serum in PBS (50 v/v%) for a specified period of time (0, 0.5, 1, 2, 4, 8, 24, and 48 h) at 37 °C under continuous shaking. At the end of each time point, the sample was mixed with proteinase K (200 μ g mL⁻¹) and frozen at -80 °C to stop the enzymatic reaction. For the analysis, samples were thawed and mixed with SDS (1.0 wt%) in order to release siRNA from the nanoparticles. The sample was then mixed with an equal amount of 2 \times loading buffer and loaded into 15% TBE-urea gel (BioRad, Hercules, CA). The gel ran at 100 V for the first 20 min, and 150 V for another hour. The gel was then stained with SyBR Gold (Life Technologies, Eugene, OR) following manufacturer's protocol, and viewed under the UV chamber. The band intensity was analyzed by ImageJ software (NIH, Bethesda, MD). The fraction of intact siRNA was reported as a function of time that the siRNA-nanoparticles were in 50% serum.

Cellular Uptake Analysis by Flow Cytometry: We conducted the cell uptake studies in cell suspension where cells were exposed to nanoparticles in three dimensions. We also used short exposure time of 0.5 and 2 h (rather than overnight exposure time as in routine transfection studies) since shorter time may better mimic in vivo exposure. However, the ratio of nanoparticle per cell was in the same par as in the routine transfection studies. Cells were harvested and resuspended in 1 \times 10⁶ cells per 150 μ L per tube. Each tube was mixed with 150 μ L of siSCR (tagged with Alexa-488)-nanoparticles in PBS (containing 100 μ g nanoparticles). Upon siSCR-nanoparticle addition, cells were placed on a rocker in the cell incubator (37 °C, 5% CO₂) for 0.5 or 2.0 h. After the specified incubation time, cells were washed (centrifuge at 115 g, 5 min) with FACS buffer (1 mL, 1 \times phosphate buffered saline (Ca/Mg++ free) + 1 \times 10⁻³ M EDTA + 25 \times 10⁻³ M HEPES pH 7.0 + 1% fetal bovine serum (heat-inactivated)) three times. Cells were then resuspended in FACS buffer (550 μ L) and transferred to 5-mL BD FACS tube. Cells were kept on ice until analysis. For cells stained with free antibody (for gating purpose), antibody labeling was performed on ice and under rocking conditions. Cells were stained with primary antibody (trastuzumab or rituximab: 2 μ g per tube) for an hour, washed (centrifuge at 115 g, 5 min) with PBS one time, stained with secondary antibody (Anti-human Alexa 488: 2 μ g per tube) for 45 min, then washed two times with PBS, and resuspended in FACS buffer (550 μ L) before analysis. All tubes were counter-stained for cellular DNA with DRAQ5 (2 μ L, 5 \times 10⁻³ M) (Cell Signaling, Danvers, MA) for 15 min on ice. Then all tubes (except antibody-labeled cells for gating purpose) were incubated with Trypan Blue (500 μ L, 0.4% in PBS) to quench fluorescence outside of the cells, and subjected to flow cytometry analysis. 10 000 events (cells) were analyzed for each sample. The intensity was processed with FlowJo software (FlowJo LLC, Ashland, OR).

In Vitro Efficacy: HER2 Protein Knockdown and Cell Viability: BT474, SKBR3, and HCC1954 were seeded in a 96-well plate for 24 h prior to

treatment. Nanoparticles were loaded with siHER2 or siSCR at NP/siRNA 50. siRNA dose was fixed at 60×10^{-9} M. Media were switched to complete media after overnight incubation. Three days after treatment with siRNA–nanoparticles, cells were fixed and analyzed for HER2 protein expression by immunofluorescence method (see details in the Supporting Information). HER2 mRNA and β -actin mRNA levels were analyzed at 48 h post-treatment using Quantigene 2.0 Reagent System (Affymetrix Panomics, Santa Clara, CA) following the manufacturer's protocol. The HER2 mRNA level was then normalized with β -actin mRNA (housekeeping gene) and reported as the percentage of the untreated control. Cell viability and apoptosis were analyzed four days post-treatment using CellTiter-Glo Luminescent Assay (Promega, Madison, WI) and Caspase-Glo 3/7 Assay Systems (Promega, Madison, WI), respectively. Caspase activity was normalized with the cell viability. Both were reported as a percentage of the untreated control.

Blood Compatibility—Hemolysis, Coagulation, and Platelet Aggregation: Studies of blood compatibility were performed following or with minor modification from the Nanotechnology Characterization Laboratory (NCL)'s published protocols. The detailed protocols can be found in the Supporting Information.

Immune Response—Peripheral Blood Mononuclear Cells (PBMCs) Cytokine Release Assay: A PBMC cytokine release assay was conducted according to the recommendations and method by the NCL of NCI for immunological studies of nanoparticles. The *in vitro* cell based assay evaluated cytokine production by PBMCs (200 000 cells/well) following a 24-h exposure to the test materials. Test materials included nanoparticles with and without siHER2 to investigate the potential impact of siRNA-mediated immune response. Following incubation, cell culture supernatants were collected and analyzed for IL-1 β , IL-6, IFN- α , and TNF- α by a cytometry bead array (Milliplex Magnetic Bead/Millipore, Billerica, MA) following manufacturer's protocol. Abraxane (Celgene, NJ) and Feraheme (AMAG Pharmaceuticals, MA) were used as FDA approved nanoparticle-based drug benchmarks since there is no siRNA-based nanoparticle drug in the market.

Animal Studies—Mouse Tumor Models and In Vivo Efficacy Studies: All animals were selected and used under an approved protocol of the Institutional Animal Care and Use Committee (IACUC) of Oregon Health and Science University. All animal experiments were carried out under the auspices of the OHSU Department of Comparative Medicine. *In vivo* gene silencing studies were performed in orthotopic mouse tumor models; HCC1954 cells (4×10^6) or JIMT-1 cells (1×10^6) unless otherwise specified were implanted into the mammary fat pads of five-week-old SCID mice (Charles River, Wilmington, MA) and allowed to grow to an average size of ≈ 250 and ≈ 150 mm³, respectively. Mice were then grouped and proceeded to receive a single injection (tail vein) of the nanoparticles (T–siHER2–NP^{10C} or T–siSCR–NP^{10C}, S-47 core, 1.25 mg siRNA kg⁻¹), or the PBS control. The tumors were harvested four days after treatment and analyzed for HER2 protein expression by immunofluorescence (Supporting Information). Subsequent study on tumor growth reduction study was also performed with the orthotopic HCC1954 tumor model. Tumors were allowed to grow to 150 mm³ prior to treatments (by tail vein injections) with siHER2 or siSCR (1.25 mg siRNA kg⁻¹ body weight) delivered with T–NP^{10C} (S-47 core) over a period of three weeks. Separate tumor growth studies were performed with free trastuzumab treatments as follows: (A) Mice ($n = 7$ /group) were injected intraperitoneally with trastuzumab (10 mg kg⁻¹) or saline. (B) Mice ($n = 5$ /group) were injected via tail vein with trastuzumab (5 mg kg⁻¹) or saline. (C) Mice ($n = 9$ /group) were injected via tail vein with trastuzumab (5 mg kg⁻¹) + paclitaxel (3.1 mg kg⁻¹) or saline. Days of injection and doses were specified in Figure 9.

Statistical Analysis: Pairwise statistical comparisons were performed using unpaired, two-tailed Student's *t* test. Tumor growth curve was analyzed with two-way ANOVA with post hoc Dunnett's multiple comparison test against the saline group. Statistical significance was established at $p \leq 0.05$. Graphpad Prism 6.0 software (GraphPad software, Inc., San Diego, CA) was utilized for statistical analyses. Unless otherwise specified, all data are presented as mean \pm SD.

Supporting Information

Supporting Information is available from the Wiley Online Library or from the author.

Acknowledgements

This work was funded by NCI/SBIR (Contract No. HHSN261201300078C), NIH/NIGMS (Grant No. R01GM089918), NIH/NIDDK (Grant No. R41DK094571), NIH/NCI (Grant No. U54CA112970), the Prospect Creek Foundation, OHSU's KCI pilot award, and OHSU's VPR fund. The authors are grateful to Prof. Rosalie Sears of OHSU for independent reviewing of the data in this paper, Dr. Lev Federov of OHSU's transgenic core for his expertise on mouse tumor models, Dr. Robert Kerbel of University of Toronto for breast cancer cell lines, Dr. Josephrajan Thainashmuthu for TEM imaging and FT-IR analysis, and Ethan Muldoon for his contribution to Figure S3A, Supporting Information. OHSU, W.N., D.J.C., J.W.G., J.M., and W.Y. have a significant financial interest in PDX Pharmaceuticals, LLC, a company that may have a commercial interest in the results of this research and technology. This potential personal and institutional conflict of interest has been reviewed and managed by OHSU. The acknowledgements were amended on March 26, 2015. A missing value was added to Table 1 on May 27, 2015.

Received: December 31, 2014

Revised: February 23, 2015

Published online: March 24, 2015

- [1] a) Cancer Genome Atlas Network, *Nature* **2012**, *490*, 61; b) D. Hanahan, R. A. Weinberg, *Cell* **2011**, *144*, 646.
- [2] a) S. M. Singel, C. Cornelius, K. Batten, G. Fasciani, W. E. Wright, L. Lum, J. W. Shay, *Clin. Cancer Res.* **2013**, *19*, 2061; b) J. A. Bauer, F. Ye, C. B. Marshall, B. D. Lehmann, C. S. Pendleton, Y. Shyr, C. L. Arteaga, J. A. Pietenpol, *Breast Cancer Res.* **2010**, *12*, R41; c) A. Ashworth, R. Bernards, *Cold Spring Harbor Perspect. Biol.* **2010**, *2*, a003327.
- [3] A. L. Hopkins, C. R. Groom, *Nat. Rev. Drug Discovery* **2002**, *1*, 727.
- [4] C. V. Pecot, G. A. Calin, R. L. Coleman, G. Lopez-Berestein, A. K. Sood, *Nat. Rev. Cancer* **2011**, *11*, 59.
- [5] K. A. Whitehead, R. Langer, D. G. Anderson, *Nat. Rev. Drug Discovery* **2009**, *8*, 129.
- [6] S. Guo, L. Huang, *J. Nanomater.* **2011**, *2011*, 12.
- [7] a) R. Kanasty, J. R. Dorkin, A. Vegas, D. Anderson, *Nat. Mater.* **2013**, *12*, 967; b) D. Haussecker, *Mol. Ther. Nucl. Acids* **2012**, *1*, e8.
- [8] a) C. Argyo, V. Weiss, C. Bräuchle, T. Bein, *Chem. Mater.* **2013**, *26*, 435; b) F. Tang, L. Li, D. Chen, *Adv. Mater.* **2012**, *24*, 1504.
- [9] a) J. Taberero, G. I. Shapiro, P. M. LoRusso, A. Cervantes, G. K. Schwartz, G. J. Weiss, L. Paz-Ares, D. C. Cho, J. R. Infante, M. Alsina, M. M. Gounder, R. Falzone, J. Harrop, A. C. S. White, I. Toudjarska, D. Bumcrot, R. E. Meyers, G. Hinkle, N. Svrcikapa, R. M. Hutabarat, V. A. Clausen, J. Cehelsky, S. V. Nochur, C. Gamba-Vitalo, A. K. Vaishnav, D. W. Y. Sah, J. A. Gollob, H. A. Burris, *Cancer Discovery* **2013**, *3*, 406; b) R. K. Ramanathan, S. I. Hamburg, M. J. Borad, M. Seetharam, M. N. Kundranda, P. Lee, P. Fredlund, M. Gilbert, C. Mast, S. C. Semple, A. D. Judge, B. Crowell, L. Vocila, I. MacLachlan, D. W. Northfelt, in *AACR 104th Annual Meeting 2013*, Washington, DC **2013**.
- [10] C. M. Rudin, J. L. Marshall, C. H. Huang, H. L. Kindler, C. Zhang, D. Kumar, P. C. Gokhale, J. Steinberg, S. Wanaski, U. N. Kasid, M. J. Ratain, *Clin. Cancer Res.* **2004**, *10*, 7244.
- [11] D. E. Fein, R. Bucki, F. Byfield, K. Leszczynska, P. A. Janmey, S. L. Diamond, *Mol. Pharmacol.* **2010**, *78*, 402.

- [12] a) M. E. Davis, J. E. Zuckerman, C. H. J. Choi, D. Seligson, A. Tolcher, C. A. Alabi, Y. Yen, J. D. Heidel, A. Ribas, *Nature* **2010**, *464*, 1067; b) M. E. Davis, *Mol. Pharm.* **2009**, *6*, 659.
- [13] J. E. Zuckerman, C. H. J. Choi, H. Han, M. E. Davis, *Proc. Natl. Acad. Sci. U.S.A.* **2012**, *109*, 3137.
- [14] J. D. Heidel, Z. Yu, J. Y.-C. Liu, S. M. Rele, Y. Liang, R. K. Zeidan, D. J. Kornbrust, M. E. Davis, *Proc. Natl. Acad. Sci. U.S.A.* **2007**, *104*, 5715.
- [15] a) Y. Ren, H. W. Cheung, G. von Maltzhan, A. Agrawal, G. S. Cowley, B. A. Weir, J. S. Boehm, P. Tamayo, A. M. Karst, J. F. Liu, M. S. Hirsch, J. P. Mesirov, R. Drapkin, D. E. Root, J. Lo, V. Fogal, E. Ruoslahti, W. C. Hahn, S. N. Bhatia, *Sci. Transl. Med.* **2012**, *4*, 147ra112; b) Y.-D. Yao, T.-M. Sun, S.-Y. Huang, S. Dou, L. Lin, J.-N. Chen, J.-B. Ruan, C.-Q. Mao, F.-Y. Yu, M.-S. Zeng, J.-Y. Zang, Q. Liu, F.-X. Su, P. Zhang, J. Lieberman, J. Wang, E. Song, *Sci. Transl. Med.* **2012**, *4*, 130ra48.
- [16] S. A. Jensen, E. S. Day, C. H. Ko, L. A. Hurley, J. P. Luciano, F. M. Kouri, T. J. Merkel, A. J. Luthi, P. C. Patel, J. I. Cutler, W. L. Daniel, A. W. Scott, M. W. Rotz, T. J. Meade, D. A. Giljohann, C. A. Mirkin, A. H. Stegh, *Sci. Transl. Med.* **2013**, *5*, 209ra152.
- [17] a) X. Li, Y. Chen, M. Wang, Y. Ma, W. Xia, H. Gu, *Biomaterials* **2013**, *34*, 1391; b) H. Meng, W. X. Mai, H. Zhang, M. Xue, T. Xia, S. Lin, X. Wang, Y. Zhao, Z. Ji, J. I. Zink, A. E. Nel, *ACS Nano* **2013**, *7*, 994; c) J. Shen, H. C. Kim, H. Su, F. Wang, J. Wolfram, D. Kirui, J. Mai, C. Mu, L. N. Ji, Z. W. Mao, H. Shen, *Theranostics* **2014**, *4*, 487; d) D. Lin, Q. Cheng, Q. Jiang, Y. Huang, Z. Yang, S. Han, Y. Zhao, S. Guo, Z. Liang, A. Dong, *Nanoscale* **2013**, *5*, 4291.
- [18] H. Maeda, J. Wu, T. Sawa, Y. Matsumura, K. Hori, *J. Controlled Release* **2000**, *65*, 271.
- [19] M. J. Roberts, M. D. Bentley, J. M. Harris, *Adv. Drug Delivery Rev.* **2002**, *54*, 459.
- [20] T. H. Chung, S. H. Wu, M. Yao, C. W. Lu, Y. S. Lin, Y. Hung, C. Y. Mou, Y. C. Chen, D. M. Huang, *Biomaterials* **2007**, *28*, 2959.
- [21] C. G. Murphy, S. Modi, *Biologics: Targets Ther.* **2009**, *3*, 289.
- [22] a) Y.-C. Wang, G. Morrison, R. Gillihan, J. Guo, R. Ward, X. Fu, M. Botero, N. Healy, S. Hilsenbeck, G. Phillips, G. Chamness, M. Rimawi, C. K. Osborne, R. Schiff, *Breast Cancer Res.* **2011**, *13*, R121; b) C. A. Ritter, M. Perez-Torres, C. Rinehart, M. Guix, T. Dugger, J. A. Engelman, C. L. Arteaga, *Clin. Cancer Res.* **2007**, *13*, 4909; c) T. Cooke, J. Reeves, A. Lanigan, P. Stanton, *Ann. Oncol.* **2001**, *12*, S23.
- [23] a) S. Ahmad, S. Gupta, R. Kumar, G. C. Varshney, G. P. S. Raghava, *Sci. Rep.* **2014**, *4*; b) R. Nahta, F. J. Esteva, *Breast Cancer Res.* **2006**, *8*, 215.
- [24] L. A. Hoeflerlin, C. E. Chalfant, M. A. Park, *J. Surg. Sci.* **2013**, *1*, 3.
- [25] a) M. Barok, H. Joensuu, J. Isola, *Breast Cancer Res.* **2014**, *16*, 1; b) A. A. Seyhan, U. Varadarajan, S. Choe, W. Liu, T. E. Ryan, *Mol. Biosyst.* **2012**, *8*, 1553.
- [26] a) T. M. Allen, P. R. Cullis, *Science* **2004**, *303*, 1818; b) H. Kobayashi, R. Watanabe, P. L. Choyke, *Theranostics* **2013**, *4*, 81.
- [27] R. A. Petros, J. M. DeSimone, *Nat. Rev. Drug Discovery* **2010**, *9*, 615.
- [28] J. Lu, M. Liong, S. Sherman, T. Xia, M. Kovichich, A. E. Nel, J. I. Zink, F. Tamanoi, *Nanobiotechnology* **2007**, *3*, 89.
- [29] O. Boussif, F. Lezoualc'h, M. A. Zanta, M. D. Mergny, D. Scherman, B. Demeneix, J. P. Behr, *Proc. Natl. Acad. Sci. U.S.A.* **1995**, *92*, 7297.
- [30] a) T. Bieber, W. Meissner, S. Kostin, A. Niemann, H. P. Elsasser, *J. Controlled Release* **2002**, *82*, 441; b) K. Kunath, A. von Harpe, D. Fischer, H. Petersen, U. Bickel, K. Voigt, T. Kissel, *J. Controlled Release* **2003**, *89*, 113; c) M. Breunig, U. Lungwitz, R. Liebl, C. Fontanari, J. Klar, A. Kurtz, T. Blunk, A. Goepferich, *J. Gene Med.* **2005**, *7*, 1287.
- [31] J. Behr, *Chimia* **1997**, *51*, 34.
- [32] H. Eliyahu, Y. Barenholz, A. J. Domb, *Molecules* **2005**, *10*, 34.
- [33] a) T.-M. Ketola, M. Hanzlíková, L. Leppänen, M. Raviña, C. J. Bishop, J. J. Green, A. Urtti, H. Lemmetyinen, M. Yliperttula, E. Vuorimaa-Laukkanen, *J. Phys. Chem. B* **2013**, *117*, 10405; b) L. Aravindan, K. A. Bicknell, G. Brooks, V. V. Khutoryanskiy, A. C. Williams, *Macromol. Biosci.* **2013**, *13*, 1163.
- [34] J. M. du Manoir, G. Francia, S. Man, M. Mossoba, J. A. Medin, A. Vilorio-Petit, D. J. Hicklin, U. Emmenegger, R. S. Kerbel, *Clin. Cancer Res.* **2006**, *12*, 904.
- [35] a) A. Mantei, S. Rutz, M. Janke, D. Kirchhoff, U. Jung, V. Patzel, U. Vogel, T. Rudel, I. Andreou, M. Weber, A. Scheffold, *Eur. J. Immunol.* **2008**, *38*, 2616; b) D. M. Dykxhoorn, D. Palliser, J. Lieberman, *Gene Ther.* **2006**, *13*, 541.
- [36] D. W. Bartlett, H. Su, I. J. Hildebrandt, W. A. Weber, M. E. Davis, *Proc. Natl. Acad. Sci. U.S.A.* **2007**, *104*, 15549.
- [37] a) Z. Zhang, A. E. Berns, S. Willbold, J. Buitenhuis, *J. Colloid Interface Sci.* **2007**, *310*, 446; b) R. Gref, M. Luck, P. Quellec, M. Marchand, E. Dellacherie, S. Harnisch, T. Blunk, R. H. Muller, *Colloids Surf., B* **2000**, *18*, 301.
- [38] S. Mao, M. Neu, O. Germershaus, O. Merkel, J. Sitterberg, U. Bakowsky, T. Kissel, *Bioconjugate Chem.* **2006**, *17*, 1209.
- [39] H. Zhang, T. Xia, H. Meng, M. Xue, S. George, Z. Ji, X. Wang, R. Liu, M. Wang, B. France, R. Rallo, R. Damoiseaux, Y. Cohen, K. A. Bradley, J. I. Zink, A. E. Nel, *ACS Nano* **2011**, *5*, 2756.
- [40] R. Nahta, *ISRN Oncol.* **2012**, *2012*, 428062.
- [41] M. H. Schwenk, *Pharmacotherapy* **2010**, *30*, 70.
- [42] K. Takeda, S. Akira, *Int. Immunol.* **2005**, *17*, 1.
- [43] a) R. Broering, C. I. Real, M. J. John, K. Jahn-Hofmann, L. M. Ickenstein, K. Kleinehr, A. Paul, K. Gibbert, U. Dittmer, G. Gerken, J. F. Schlaak, *Int. Immunol.* **2014**, *26*, 35; b) M. Zamanian-Daryoush, J. T. Marques, M. P. Gantier, M. A. Behlke, M. John, P. Rayman, J. Finke, B. R. Williams, *J. Interferon Cytokine Res.* **2008**, *28*, 221.
- [44] A. Chaturvedi, S. K. Pierce, *Traffic* **2009**, *10*, 621.
- [45] R. M. Crist, J. H. Grossman, A. K. Patri, S. T. Stern, M. A. Dobrovolskaia, P. P. Adisheshaiah, J. D. Clogston, S. E. McNeil, *Integr. Biol.* **2013**, *5*, 66.
- [46] I. Beyer, H. Cao, J. Persson, H. Song, M. Richter, Q. Feng, R. Yumul, R. van Rensburg, Z. Li, R. Berenson, D. Carter, S. Roffler, C. Drescher, A. Lieber, *Clin. Cancer Res.* **2012**, *18*, 3340.
- [47] I. Beyer, Z. Li, J. Persson, Y. Liu, R. van Rensburg, R. Yumul, X. B. Zhang, M. C. Hung, A. Lieber, *Mol. Ther.* **2011**, *19*, 479.
- [48] F. Henjes, C. Bender, S. von der Heyde, L. Braun, H. A. Mannsperger, C. Schmidt, S. Wiemann, M. Hasmann, S. Aulmann, T. Beissbarth, U. Korf, *Oncogenesis* **2012**, *1*, e16.
- [49] a) L. Pan, Q. He, J. Liu, Y. Chen, M. Ma, L. Zhang, J. Shi, *J. Am. Chem. Soc.* **2012**, *134*, 5722; b) I. I. Slowing, B. G. Trewyn, S. Giri, V. S. Y. Lin, *Adv. Funct. Mater.* **2007**, *17*, 1225.
- [50] a) P. Yousefpour, F. Atiyabi, E. Vasheghani-Farahani, A. A. Movahedi, R. Dinarvand, *Int. J. Nanomed.* **2011**, *6*, 1977; b) M. N. Koopaei, R. Dinarvand, M. Amini, H. Rabbani, S. Emami, S. N. Ostad, F. Atiyabi, *Int. J. Nanomed.* **2011**, *6*, 1903.